J. Geotech. Eng., JSCE, No. 624/III-47, 1-10, 1999 June

FRACTURE SIMULATIONS USING MANIFOLD AND SINGULAR BOUNDARY ELEMENT METHOD

Guo-Xin ZHANG[1], Yasuhito SUGIURA[2] and Hiroo HASEGAWA[3]

[1]Dr. Eng., River Technology Department, I.N.A. Corporation (Sekiguchi 1-44-10, Bunkyo-ku, Tokyo, 112-8668, Japan)
[2]M. Eng., River Technology Department, I.N.A. Corporation (Sekiguchi 1-44-10, Bunkyo-ku, Tokyo, 112-8668, Japan)
[3]M. Eng., River Technology Department, I.N.A. Corporation (Sekiguchi 1-44-10, Bunkyo-ku, Tokyo, 112-8668, Japan)

A second-order manifold method has been developed and is described. By means of a singular boundary element method proposed by the author, the failure process of a structure can be numerically analyzed. Mohr-Coulomb's law is employed as a criterion for new crack initiation and maximum circumferential stress theory is used as a criterion for the propagation of existing cracks. Comparison of the computed stress intensity factor with results obtained via the collocation method demonstrates the high predictive accuracy of the present method. Examples of our present method applied to static and dynamic problems are presented.

Key Words: manifold method, crack propagation, boundary element method

1. INTRODUCTION

Several numerical methods are available for simulating crack propagation and the failure of structures with discontinuities. These methods include the Finite Element Method (FEM), the Boundary Element Method (BEM), the Discrete Element Method (DEM) and the Discontinuous Displacement Analysis (DDA). Although the FEM and the BEM using fine meshes with special elements can model crack propagation and the failure of structures, it is difficult to describe the discontinuities after cracks begin propagating, and small deformation restrictions are usually needed. Also the number of cracks that can be handled is limited. Therefore the behavior of failed structures and problems involving many discontinuities cannot be readily analyzed. The DEM and DDA can be utilized to model the behavior of discontinuities or block systems, but the stress distribution inside the blocks cannot be calculated properly, hence the propagation of cracks through the blocks cannot be well modeled.

Proposed by Shi[1), 2)], the Manifold Method (MM) is a new numerical tool for solving problems involving both continuous and discontinuous media. By introducing the concept of a cover and two sets of meshes, the manifold method combines the advantages of the FEM and DDA. It can deal with not only discontinuities, contact, large scale deformation and block movement as does the DDA, but also the stress distribution within each block as accurately as does the FEM.

To simulate crack initiation and propagation by the manifold method, Zhang et al[3), 4)] have extended the original MM by using the Mohr-Coulomb's law to determine the fracture criterion. But a misevaluation may occur on account of the stress concentration near the crack tip. Because the stress at the crack tip is always infinite even for a small load (in the brittle fracture problem), the crack may continue propagating indefinitely when the meshes are fine enough if the Mohr-Coulomb's criterion is utilized. Chiou et al[5)] have calculated the Stress Intensity Factor (SIF) using fine meshes near the crack tip and have also used a maximum circumferential stress criterion to simulate crack propagation. But the meshes must be refined constantly with the propagation of cracks, which may interrupt the computation because of the distortion of the elements.

In this paper we propose a method that combines the second order MM and the singular BEM to simulate crack initiation and subsequent propagation. The stress and displacement fields are calculated via the second order MM; the SIF at the crack tip is computed using the singular BEM. The Mohr-Coulomb's fracture criterion is only used to

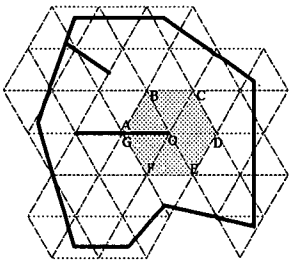

(a) Structure with discontinuities.

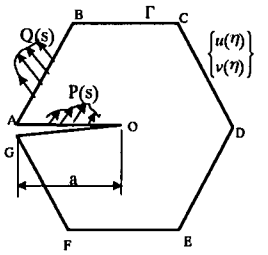

(b) Sub-region containing a crack.

Fig. 1 Structure containing cracks and an enlarged sub-region.

locate the initial crack; for analyzing its subsequent propagation the stress intensity factor is the criterion used. Numerical examples are given to illustrate application of this method.

The numerical procedure for simulating crack propagation is as follows: Firstly, calculate the displacement and stresses of a structure {**Fig. 1 (a)**} with discontinuities including joints and cracks using the second order manifold method. Secondly, specify a sub-region including at least one crack tip as a specific problem, solve this problem using the singular BEM. In doing this, the displacement obtained by manifold method along the boundary of sub-region is taken as the restraint conditions, and the traction free condition on the crack surface is considered {**Fig. 1 (b)**}. Finally, calculate the SIF at the crack tip, judge the crack to be propagating or not, reform the mathematical and physical meshes as needed and recalculate, and then move to the next region.

2. STRUCTURE ANALYSIS BY MM

(1) Basic concepts of MM

a) Cover and two sets of meshes

The manifold method uses the concept of cover and two sets of meshes. Cover is used to define the local function that will be described in the next section. Every cover overlays a fixed area, the size and shape of this area can be chosen arbitrarily depending on the problem to be solved. The covers

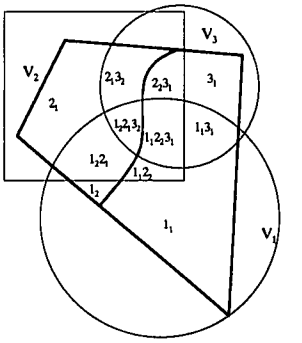

Fig. 2 General covers with one joint.

overlap one another and overlay the entire physical domain.

The two sets of meshes are the physical meshes and mathematical meshes. The physical meshes describe the physical domain (including boundaries, joints and the interfaces between blocks) and define the integration areas. The physical meshes are definitively determined by the problem being analyzed. The mathematical meshes, on the other hand, are enclosed lines more or less arbitrarily selected for the problem. The areas enclosed by the mathematical meshes are called the mathematical covers, on which the space function is built. The mathematical meshes should be large enough to cover every point of the physical meshes.

The physical and mathematical meshes intersect each other and form physical covers. If the physical meshes divide a mathematical cover into two or more completely disconnected regions, each of these regions is called a physical cover.

All of the enclosed areas generated by the intersection between physical meshes and mathematical meshes are defined as elements. Elements can have any shape. One or more physical covers may overlay an element. All of an element's covers determine its behavior.

Figure 2 gives an example of general covers of the MM in blocks with one joint[2]. Two circles and one rectangle (thin lines) delimit three mathematical covers V_1, V_2 and V_3 to form mathematical meshes. The physical meshes (thick lines) divide V_1, into two physical covers 1_1 and 1_2; V_2, into two physical covers 2_1 and 2_2; and V_3, into two physical covers 3_1 and 3_2. Eleven computational elements are generated by the intersection of the two sets of meshes and are denoted in this figure as 1_1, $1_1 2_2$, $1_1 2_2 3_1$, $1_2 2_1 3_2$, etc.

The meshes of the FEM can be used to define covers for the MM. For any node, all elements having this node form a mathematical cover. For three node triangular meshes, three covers overlay

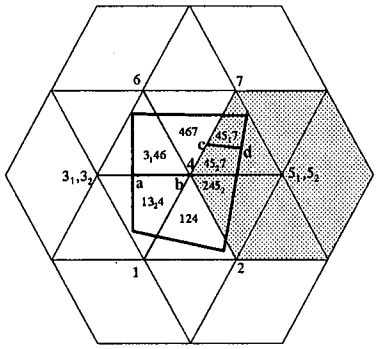

Fig. 3 FEM-type covers of the Manifold Method in one block with two joints.

every element. For six node triangular meshes, six covers overlay every element. **Figure 3** shows an example of FEM type covers. Seven hexagonal mathematical covers around seven points, labeled 1-7 in **Fig. 3**, are apparent and formed by the thin lines. The physical meshes (formed by thick lines – one block with two joints a-b and c-d) divide the mathematical cover around point 3, into two physical covers 3_1 and 3_2, and divide the mathematical cover around point 5, into two physical covers 5_1 and 5_2. Nine physical covers (1,2,3_1,3_2,4, etc) and seven computational elements (124, 245_2, 45_27, etc) are generated.

b) Local function and global function

For each cover, a local function can be defined, and these local functions can be combined using a weighting function to form a global function that defines the displacement and stress in the whole region. If the local cover function $u_i(x,y)$ is defined for a physical cover U_i as:

$$u_i(x,y) \qquad (x,y) \in U_i,$$

then the global function $u(x,y)$ for the whole physical cover system can be expressed as:

$$u(x,y) = \sum_1^n w_i(x,y) u_i(x,y) \tag{1}$$

where $w_i(x,y)$ is weight function defined as:

$$w_i(x,y) \geq 0 \quad (x,y) \in U_i$$
$$w_i(x,y) = 0 \quad (x,y) \notin U_i$$
$$with \quad \sum_{(x,y) \in U_i} w_i = 1.$$

With the cover concept and the definitions of local and global functions, the MM can model a wide variety of continuous and discontinuous structures. The FEM and DDA can be regarded as special cases of it.

c) Simultaneous equilibrium equations

If the local displacement function for each physical cover is assumed to be constant, that is, the local displacement function for cover U_i reads:

$$u_i(x,y) = \begin{Bmatrix} u_i \\ v_i \end{Bmatrix} = \{D_i\}$$

then the simultaneous equilibrium equation takes the form:

$$\left\{\alpha \frac{2}{\Delta t^2}[M] + \alpha \frac{2}{\Delta t}[C] + [K]\right\}\{\Delta D\} = \beta \frac{2}{\Delta t}[M]\{\dot{D}\} + [\Delta F] \tag{2}$$

where Δt is a time step, $[M]$ is the inertia matrix, [C] is the viscosity matrix, $[K]$ is the global stiffness matrix (including element stiffness, penetration of the contact point and the stiffness of the fixed point), $\{\Delta D\}$ is the increment of displacement, $\{\dot{D}\}$ is the velocity vector, $\{\Delta F\}$ is the load increment including initial stress, body force, point load, bonding force and penetration force of contact, α and β are parameters defined as below:

$\alpha = \beta = 1$, for dynamic problems,
$\alpha = 0$, $\beta = 1$, for static problems.

A detailed discussion of Eq. (2) can be found in papers reported by Shi[1), 2)].

(2) Second-order MM

The original first-order MM uses the constant cover displacement $u_i(x,y)$ and the linear weight function $w_i(x,y)$ to construct the global displacement function. Use of a linear global function reduces the accuracy of the MM in simulating crack propagation. To increase the predictive accuracy a second-order MM is introduced here by constructing a second-order global function.

A second-order displacement function can be built in either of two ways: (a) the linear weight function $w_i(x,y)$ and the linear cover function $u_i(x,y)$, (b) the second-order weight function $w_i(x,y)$ and the constant cover function $u_i(x,y)$. We follow the latter one here and consider the six node finite elements forming the mathematical meshes. The second-order weight function is:

$$w_i(x,y) = f_{i1} + f_{i2}x + f_{i3}y + f_{i4}x^2 + f_{i5}xy + f_{i6}y^2 \qquad (i = 1, 2 \cdots 6). \tag{3}$$

The global function to second-order is Eq. (3) together with Eq. (1) for the constant local function $u_i(x,y)$.

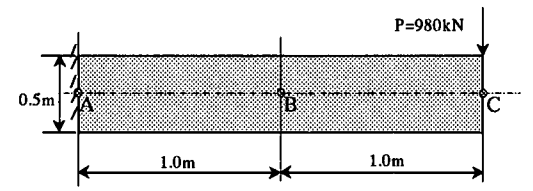

(a) Cantilever with point load.

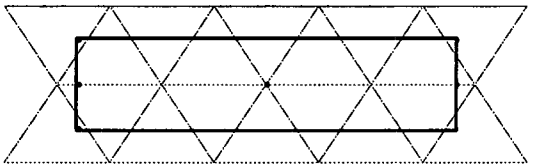

(b) Physical meshes (thick lines) and mathematical meshes (thin lines).

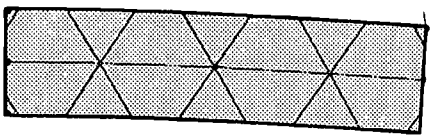

(c) Original MM.

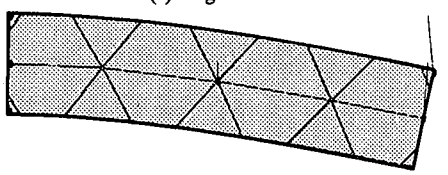

(d) Second order MM.

Fig. 4 Deformation of cantilever by the Manifold Method.

Table 1 Comparison of computed displacements with analytical solutions.

Displacement	Analytical (mm)	First Order MM (mm)	Second Order MM (mm)
A	0	0	0
B	84	23	84.4
C	264	85	266.8

A computational example is given here to compare the predictive performance of the original MM and our second-order MM. **Figure 4(a)** shows a 2m×0.5m cantilever loaded by P = 980 kN. The Young's modulus and Poisson's ratio for the cantilever are 98 MPa and 0.24, respectively. Computed displacements at points A, B and C are compared with the analytical solutions in **Table 1**. The calculation meshes and the deformations of the cantilever by the first-order MM and the second-order MM are shown in **Fig. 4{(b)–(d)}**. The results confirm a drastic improvement in predictive accuracy with the second order MM.

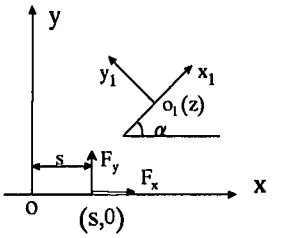

Fig. 5 Infinite plane with point load at (s, 0).

(3) Unique features of MM

As a generalization of the FEM and DDA, the manifold method differs from the FEM as follows: (a) The manifold method utilizes mathematical and physical meshes; the FEM can be understood as a special case of the manifold method that combines both sets of meshes. (b) Unknown variables are defined at the nodes of the mathematical meshes (covers). These nodes can be outside of the physical domain (material region). The grouped integration area for the mathematical and physical meshes can have any shape and simplex integration[2] (analytical integration) is used with the MM, whereas the FEM involves numerical integration such as Gauss integration. (c) The MM employs a "Penalty" (by adding a hard spring) to deal with the contact of discontinuities; it facilitates the analysis of discontinuous problems/the block system. (d) With the MM, the nodes of the mathematical meshes and the vertices of physical meshes are adjusted at every step of the calculation, which simplifies the handling of large-scale deformations and the movement of blocks. (e) In simulating static problems, setting β = 1 in the equilibrium Eq. (2) allows the MM algorithm to continue computation after the initial structural failure, while the FEM computation cannot be continued once the structure initially fails.

3. SUB-REGION ANALYSIS USING SINGULAR BEM

The sub-region with a crack **{Fig. 1(b)}** and the known boundary displacement $u(\eta), v(\eta)$ can be regarded as a boundary value problem and can be solved by an indirect boundary element method. In order to form the integral equations, necessary for solving the problem, two kinds of fundamental solutions are required.

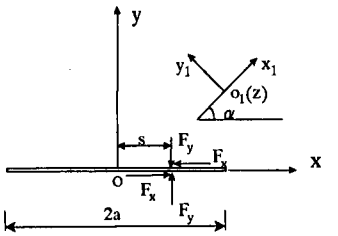

Fig. 6 Infinite plane with crack, and the point load $P = F_y\text{-}iF_x$

(1) Static mechanical fundamental solution for an infinite continuous region

When a complex point force $Q = \dfrac{F_x + iF_y}{2\pi(1+\kappa)}$ is applied at point z = s on a complex plane (**Fig. 5**), the stresses and displacements in the x_1–y_1 coordinate system which makes an angle α with the x direction at point z can be obtained from the Kelvin solution[6]:

$$\sigma^{*(1)}_{y_1} - i\tau^{*(1)}_{x_1y_1} = -Q\left[\frac{1}{z-s} - \kappa e^{-2i\alpha}\frac{1}{\bar{z}-s}\right] - \bar{Q}\left[\frac{1}{\bar{z}-s} - e^{-2i\alpha}\frac{(z-s)}{(\bar{z}-s)^2}\right] \tag{4}$$

$$\sigma^{*(1)}_{x_1} + \sigma^{*(1)}_{y_1} = -2Q\frac{1}{z-s} - 2\bar{Q}\frac{1}{\bar{z}-s}$$

$$u_1^{*(1)} + v_1^{*(1)} = \frac{e^{-i\alpha}}{2\mu}\left\{-\kappa Q[\ln(z-s) + \ln(\bar{z}-s) + 1] + \bar{Q}\frac{z-s}{\bar{z}-s}\right\}$$

where μ is the shear modulus, κ = 3-4ν for the plane strain and $\kappa = (3\text{-}\nu)/(1+\nu)$ for the plane stress.

(2) Fundamental solution of a point force on crack surface

In order to fix the singularity at the crack tip, a singular fundamental solution should be used. For an infinite region with a crack of length 2a subjected to a paired point force $P = F_y\text{-}iF_x$ at z = s, as shown in **Fig. 6**, the stresses and displacements in the x_1–y_1 coordinate system can be obtained by solving the Cauchy problem[7]:

$$\sigma^{*(2)}_{y_1} - i\tau^{*(2)}_{x_1y_1} = PC(z,a,s,\alpha) + \bar{P}D(z,a,s,\alpha)$$

$$\sigma^{*(2)}_{x_1} + \sigma^{*(2)}_{y_1} = -2\frac{\sqrt{a^2-s^2}}{\pi}\mathrm{Re}\left[\frac{P}{(z-s)\sqrt{z^2-a^2}}\right] \tag{5}$$

$$u_1^{*(2)} + v_1^{*(2)} = \frac{e^{-i\alpha}}{4\pi\mu}\left\{\begin{matrix} P[\bar{f}_1(z,a,s) - \kappa f_1(z,a,s)] \\ +\bar{P}(z-\bar{z})\sqrt{a^2-s^2}\,\overline{G(z,a,s)}\end{matrix}\right\}$$

where:

$$G(z,a,s) = \frac{1}{(z-s)\sqrt{z^2-a^2}}$$

$$f_1(z,a,s) = i\left[\begin{matrix}\ln\left(\dfrac{\sqrt{z^2-a^2}+i\sqrt{a^2-s^2}}{z-s} - \dfrac{is}{\sqrt{a^2-s^2}}\right) \\ -\ln\left(1+\dfrac{s}{\sqrt{s^2-a^2}}\right)\end{matrix}\right]$$

$$C(z,a,s,\alpha) = -\frac{1}{2\pi}\sqrt{a^2-s^2}\left[G(z,a,s) + e^{-2i\alpha}\overline{G(z,a,\alpha)}\right]$$

$$D(z,a,s,\alpha) = -\frac{1}{2\pi}\sqrt{a^2-s^2}\left[\begin{matrix}\overline{G(z,a,s)}(1-e^{-2i\alpha}) \\ +e^{-2i\alpha}(z-\bar{z})\overline{G'(z,a,\alpha)}\end{matrix}\right].$$

(3) Boundary integral equations

Returning to the sub-region problem shown in **Fig. 1(b)**, we assume a distributed fictitious force $Q(s)$ is applied to the boundary Γ and the fictitious force $P(s)$ acts on the crack surface. The stresses and displacements at point z in the sub-region can be defined by integrating Eqs. (4) and (5):

$$\begin{aligned}
u_1(z,\alpha) + iv_1(z,\alpha) &= \int_\Gamma \{u_1^{*(1)}[Q(s),z,\alpha] + iv_1^{*(1)}[Q(s),z,\alpha]\}ds \\
&+ \int_{-a}^{a}\{u_1^{*(2)}[P(s),z,\alpha] + iv_1^{*(2)}[P(s),z,\alpha]\}ds \\
\sigma_{x_1}(z,\alpha) + \sigma_{y_1}(z,\alpha) &= \int_\Gamma \{\sigma_{x_1}^{*(1)}[Q(s),z,\alpha] + \sigma_{y_1}^{*(1)}[Q(s),z,\alpha]\}ds \\
&+ \int_{-a}^{a}\{\sigma_{x_1}^{*(2)}[P(s),z,\alpha] + \sigma_{y_1}^{*(2)}[P(s),z,\alpha]\}ds \\
\sigma_{x_1}(z,\alpha) - i\tau_{x_1y_1}(z,\alpha) &= \int_\Gamma \{\sigma_{x_1}^{*(1)}[Q(s),z,\alpha] - i\tau_{x_1y_1}^{*(1)}[Q(s),z,\alpha]\}ds \\
&+ \int_{-a}^{a}\{\sigma_{y_1}^{*(2)}[P(s),z,\alpha] - i\tau_{x_1y_1}^{*(2)}[P(s),z,\alpha]\}ds.
\end{aligned} \tag{6}$$

Suppose the displacement on boundary Γ calculated by the MM is $\bar{u}(\eta) + i\bar{v}(\eta)$, where $\bar{u}(\eta)$ and $\bar{v}(\eta)$ denote the normal and tangential displacements at point η on Γ. Let point z in the first formula of Eq. (6) approach the point η on the boundary Γ, i.e., $\bar{u}(\eta) + i\bar{v}(\eta) = (u(z) + iv(z))\big|_{z\to\eta}$, an integral equation that satisfies the known displacement condition on Γ can be obtained:

$$\begin{aligned}
&\int_\Gamma \{u_1^{*(1)}[Q(s),\eta,\beta_\eta] + iv_1^{*(1)}[Q(s),\eta,\beta_\eta]\}ds \\
&+ \int_{-a}^{a}\{u_1^{*(2)}[P(s),\eta,\beta_\eta] + iv_1^{*(2)}[P(s),\eta,\beta_\eta]\}ds = \bar{u}(\eta) + i\bar{v}(\eta).
\end{aligned} \tag{7a}$$

Another integral equation, which satisfies the traction free condition on the crack surface, can be obtained by letting point z in the third formula of Eq. (6) approach the point ξ on the crack surface in

a similar way:

$$P(\xi)+\int_{\Gamma}\left\{\sigma_{y_1}^{*(1)}\left[Q(s),\xi,\beta_{\xi s}\right]-i\tau_{x_1y_1}^{*(1)}\left[Q(s),\xi,\beta_{\xi s}\right]\right\}ds+ \int_{-a}^{a}\left\{\sigma_{y_1}^{*(2)}\left[P(s),\xi,\beta_{\xi s}\right]-i\tau_{x_1y_1}^{*(2)}\left[P(s),\xi,\beta_{\xi s}\right]\right\}ds=0+i0 \quad (7b)$$

where $\beta_{\eta s}=\alpha_{\eta}-\alpha_{s}$.

Solving Eq. (7) by the boundary element method yields solutions for $Q(s)$ and $P(s)$. The stress intensity factors K_I and K_{II} at the crack tip can then be calculated from Eq. (8) [8]:

$$K_{\mathrm{I}}-iK_{\mathrm{II}}=-\frac{1}{\sqrt{\pi a}}\int_{-a}^{a}P(s)\sqrt{\frac{a+s}{a-s}}ds\ . \quad (8)$$

In calculating the SIF using a traditional numerical method like the FEM, fine meshes near the crack tip are usually necessary in order to capture the stress concentration there. But actually the singular area is restrained to a small region near the crack tip, and its influences on the stress and displacement in the far area are not significant. In the present method, the stress and displacement are firstly calculated by the second-order manifold method and their precision far from the crack tip can be ensured. Then the SIF is computed by the singular BEM based on the stress and displacement obtained. Therefore higher accuracy in the calculation of the SIF can be ensured even when relatively coarse meshes are used near the crack tip.

4. CRACK MODELING

Fracture criteria using the SIF can only be used for existing cracks. For the initiation of new cracks, a stress-based criterion should be considered. In this paper, Mohr-Coulomb's law with three parameters is taken as the failure criterion for new cracks. It is assumed that new cracks start appearing if: (a) the first principle stress is larger than the tensile strength of the material, or (b) the maximum shear stress is larger than the shear strength of the material. Take σ_1 and σ_3 to indicate the first and third principal stresses, the failure criterion can then be expressed as:

Tensile failure:

$$\sigma_1=T_0.$$

Shearing failure:

$$\frac{(\sigma_1-\sigma_3)}{2}=C \qquad if\ \frac{(\sigma_1+\sigma_3)}{2}>0\ and\ 0<\sigma_1<T_0,$$

$$\frac{(\sigma_1-\sigma_3)}{2}=C\cos\phi-\frac{(\sigma_1+\sigma_3)}{2}\sin\phi \qquad if\ \frac{(\sigma_1+\sigma_3)}{2}<0\ and\ 0<\sigma_1<T_0, \quad (9)$$

where T_0 is the tension strength of the material, C is the cohesion and ϕ is the friction angle.

The maximum circumferential stress theory [9] is taken as the criterion for simulating the propagation of existing cracks. This theory supposes that the cracks propagate along the direction of maximum circumferential stress near the crack tip if this stress is larger than the critical value. Based on well-known principles of fracture mechanics, the circumferential stress σ_θ near the crack tip can be expressed by stress intensity factors in the form [10]:

$$\sigma_\theta=\frac{1}{\sqrt{2\pi r}}\cos\frac{\theta}{2}\left(K_{\mathrm{I}}\cos^2\frac{\theta}{2}-\frac{3}{2}K_{\mathrm{II}}\sin\theta\right)\ . \quad (10)$$

The crack propagation direction θ_0 is obtained by performing $\partial\sigma_\theta/\partial\theta_{|\theta=\theta_0}=0$:

$$K_I\sin\theta_0+K_{II}(3\cos\theta_0-1)=0\ . \quad (11)$$

The maximum circumferential stress σ_{θ_0} is then obtained from Eq. (10).

The critical circumferential stress $(\sigma_\theta)_c$ is a material-dependent property and can be determined as a special case. For a first mode fracture problem, $K_{II}=0$ and $\theta_0=0$, then $(\sigma_\theta)_c$ can be expressed as:

$$(\sigma_\theta)_c=\frac{K_{IC}}{\sqrt{2\pi r}}\ . \quad (12)$$

Substituting Eq. (12) into Eq. (10) yields the fracture criterion for the mixed mode fracture problem as:

$$\cos\frac{\theta_0}{2}\left(K_{\mathrm{I}}\cos^2\frac{\theta_0}{2}-\frac{3}{2}K_{\mathrm{II}}\sin\theta_0\right)=K_{IC}\ . \quad (13)$$

We now have two fracture criteria, Eq. (9) for the onset of new cracks and Eq. (13) for the propagation of exiting cracks. For dynamic problems, however, Eq. (9) is also used for judging the propagation of existing cracks as a compromise method in the present study. Since multi-crack propagation and branching are always accompanied by dynamic fractures, the single crack-based criterion {Eq. (13)} may not be directly applied.

The present research assumes no energy loss in the fracture process, that is, the total energy of the cover before fracture has to equal the energy of the two covers after the fracture. In order to ensure energy conservation during fracture, new-formed covers are forced to have the same velocity, stresses and coordinate as the original ones. Consider a cover i, which is fractured into covers i_1 and i_2 at a certain time, the total energy of this cover before and after fracture can be expressed as:

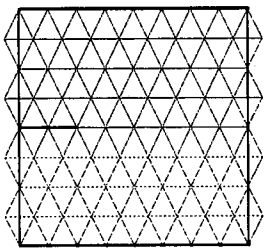

Fig. 7 Meshes used in the analysis of rectangular plate.

$$E_{old} = \frac{1}{2}m_i\dot{D}_i^{\,2} + \frac{1}{2}\sigma_i\varepsilon_i V_i$$

$$E_{new} = \frac{1}{2}m_{i1}\dot{D}_{i1}^{\,2} + \frac{1}{2}\sigma_{i1}\varepsilon_{i1}V_{i1} + \frac{1}{2}m_{i2}\dot{D}_{i2}^{\,2} + \frac{1}{2}\sigma_{i2}\varepsilon_{2i}V_{i2} \qquad (14)$$

where m is the mass of cover i, $m_i=m_{i1}+m_{i2}$, V is the volume cover, $V_i=V_{i1}+V_{i2}$. $\dot{D}_i$ is the velocity of the original cover, $\dot{D}_{i1}$ and $\dot{D}_{i2}$ are the velocities of new covers i_1 and i_2.

Because $\dot{D}_{i1} = \dot{D}_{i2}=\dot{D}_i$ and $\sigma_{i1}=\sigma_{i2}=\sigma_{i1}$, the energy conservation can be ensured.

5. APPLICATION EXAMPLES

Applications of the method developed here are presented in this section for calculating the SIF of cracks in a rectangular plate and for simulating both static {examples (2)~(4)} and dynamic problem {example (5)} of structural failure. Theoretically, cracks may initiate and propagate in any direction in spite of the arrangement of the meshes; however, for all applied examples presented here the cracks are assumed to initiate and propagate along the edge of the mathematical meshes for considerably simplifying the programming.

(1) SIF of edge crack and central crack in rectangular plate

In the first example, we compute the SIF of the edge and central cracks in a rectangular plate to examine the accuracy of the method. The results are compared with the collocation method[11]. **Figure 7** shows the meshes used in the calculation. The results are given in **Fig. 8**. It can be seen that the SIF calculated by the present method agrees quite well with that obtained via the collocation method. For the central crack with a/w = 0.25 the error is less than 5.5% although only two elements are set on the crack. Further calculation shows that the error reduces to less than 0.5% if four elements are used for the crack.

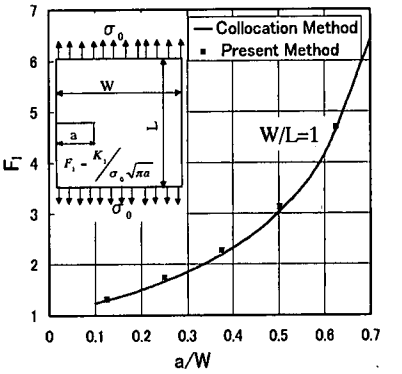

(a) SIF of an edge crack.

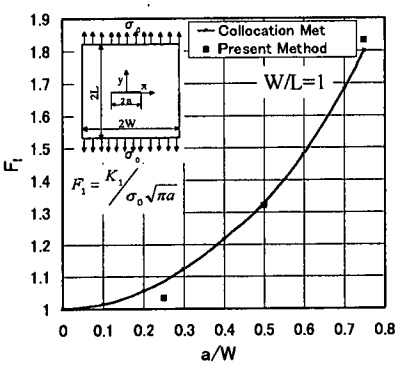

(b) SIF of a central crack.

Fig. 8 Stress Intensity Factor (SIF) of cracks in rectangular plate.

Table 2 Material properties and calculation conditions.

Elastic Modulus	19600 MPa
Poisson's Ratio	0.24
Fracture Toughness	490 N/cm$^{3/2}$
Unit Mass	23.52kN/m^3
Tension Strength T_0	0.98 MPa
Cohesion C	2.94 MPa
Friction Angle ϕ	30 degree
Calculation Mode	Static
Penalty	4900000000 kN/m

(2) Failure of block with point-loaded edge crack

This example simulates crack propagation in a 2m×2m block with a 1m long crack. A load of H = 980 kN acts horizontally. **Figure 9(a)** shows a diagram of the block and load. The material properties and calculation conditions are listed in **Table 2**.

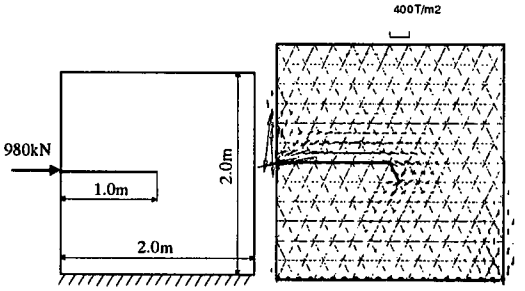

(a) shape and load. (b) beginning of propagation.

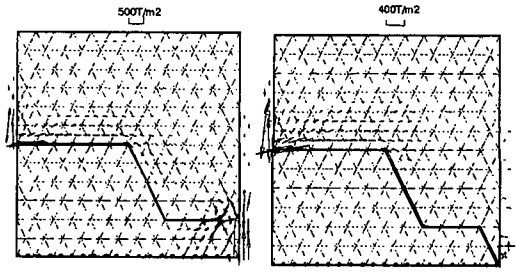

(c) new crack initiation. (d) crack penetration.

Fig. 9 Stress distribution and crack propagation in block.

Figure 9 depicts the principal stress field and the crack propagation process in the block. In the calculation, the load H is divided into 10 sequential steps. With each step, an additional 98 kN load is added. For the first and second (loading) steps, the stresses in the block and the SIF at the crack tip are not large enough to initiate new cracks or propagate existing cracks. At the third step, the SIF at the crack tip reaches the fracture criterion {Eq. (13)}. The crack starts propagating **{Fig. 9(b)}** in a direction that is about 70 degrees with the horizontal. The crack continues propagating and changes its propagation direction and finally penetrates the whole block **{Fig. 9[(c) and (d)]}**.

(3) Failure of three point bending beam

A beam with a vertical load P = 490 kN at the central point of its upper surface is shown in **Fig. 10**. The Young's modulus and Poisson's ratio of the beam are 19600 MPa and 0.2 respectively. The unit weight of material is 19.6 kN/m^3. Other parameters and computational conditions are the same as that used in the previous example. The static mode is also used in this example. The load P is subdivided into ten loading steps. The principal stress distribution, the crack propagation and the displacement of the beam at loading step 3 are shown in **Fig. 11**.

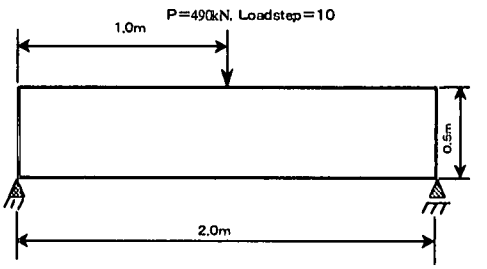

Fig. 10 Three-point bending beam.

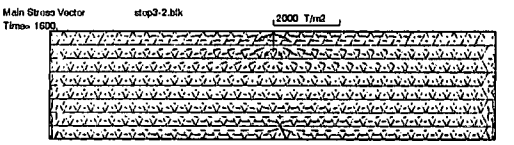

(a) Crack initiation.

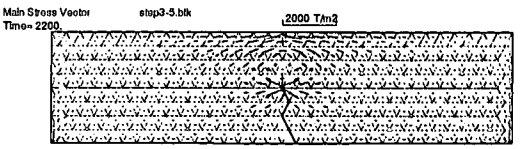

(b) Crack propagation.

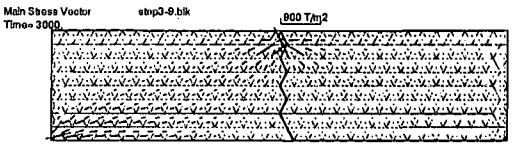

(c) Crack penetration.

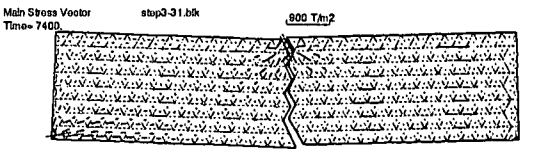

(d) Beam deformation.

Fig. 11 Principal stress distribution and crack propagation in three point bending beam.

Figure 11 shows that the stress is concentrated near the two restraint points and the loading point. The maximum tensional stress occurs at the middle of the lower beam surface. At the third (loading) step, the maximum tensional stress reaches the failure criterion and a new crack starts forming in the middle of the beam's lower surface **{Fig. 11(b)}**. The crack propagates until the beam ruptures **{Fig. 11(c)}**. The direction of crack propagation is nearly along the vertical. Computations show that under the given conditions, the bearing capacity of the beam is less than 294 kN. Continued additions to the load result in movement of the broken blocks as shown in **Fig. {11(d)}**.

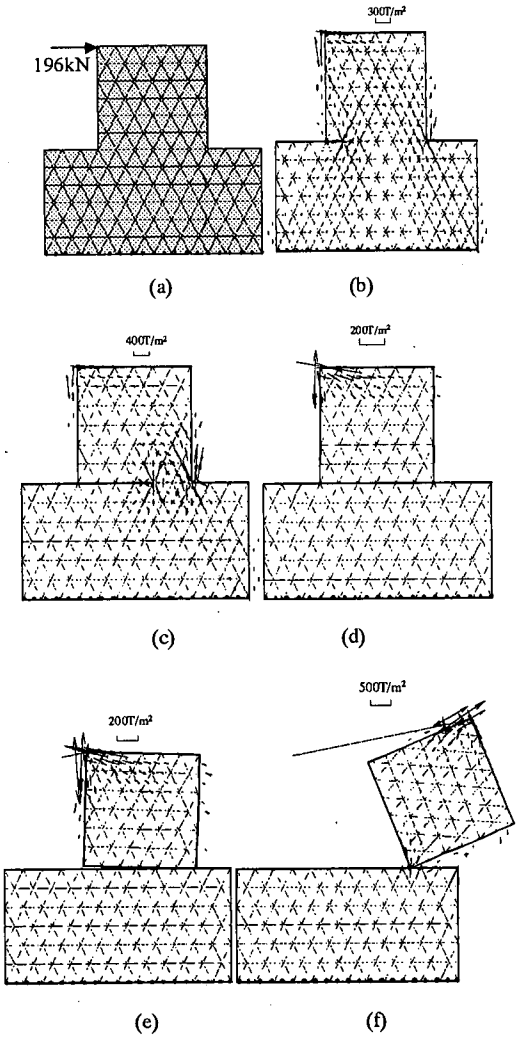

Fig. 12 Structural failure and block movement.

(4) Failure of structure and the movement of blocks

Figure 12 shows another computational example of the failure of a structure and the movement of blocks. The structure is loaded by a horizontal point load P = 196 kN. The load P is subdivided into four loading steps for the calculation. At the third loading step, the crack begins to form at the left corner **{Fig. 12(b)}**. The crack propagates into the structure until the structure is broken into two blocks **[Fig. 12{(c)-(d)}]**. The upper block starts to move with a continued application of the load **[Fig. 12{(e)-(f)}]**.

(5) Arch failure by a hitting load

As an example of the modified MM applied to a dynamic problem, the failure of an arch hit by a flying object has been simulated.

Table 3 Material properties and calculation conditions.

	Abutment	Arch
Elastic Modulus	1960 MPa	1960 MPa
Poisson's Ratio	0.24	0.24
Unit Mass	23.52kN/m^3	23.52kN/m^3
Tension Strength T_0	9800 MPa	0.01 MPa
Cohesion C	29400 MPa	0.03 MPa
Friction Angle ϕ	30 degree	10 degree
Calculation Mode	dynamic	dynamic
Penalty	98000000 kN/m	98000000 kN/m

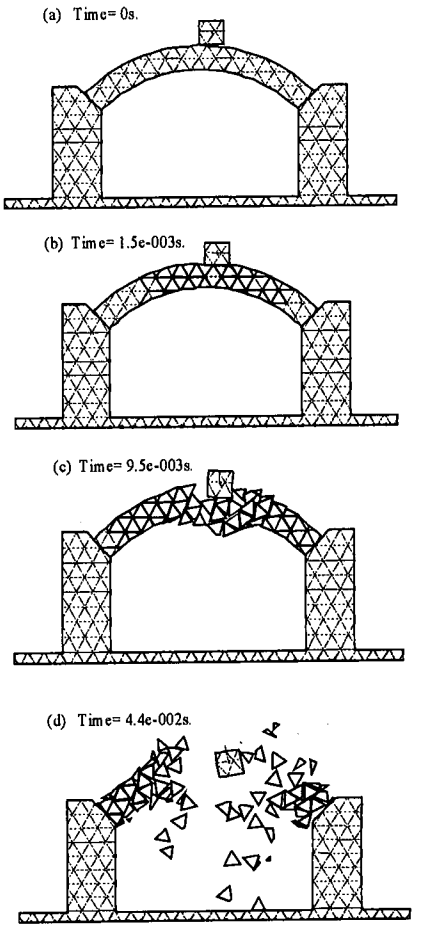

Fig. 13 Arch failure process.

Figure 13(a) shows the analysis domain with a thick line indicating the boundary and physical joints and a thin line the mathematical meshes in the simulation. The bottom of the structure is fixed. The material of the arch and abutments is the same, but the strength of the abutments has an extremely high value so that the cracks can only form and propagate within the arch. The material properties and numerical parameters are listed in **Table 3**. The

velocity of the flying block is $v_x = 0$, $v_y = -140$ m/s.

Figure 13 {(b)–(d)} illustrates the time evolution of the failure process for the arch. The object hits the arch (at time t = 0), cracks initiate near the percussion point and rapidly propagate along two sides. By t = 0.0095 second, almost all the elements have failed, and in a very short time the arch collapses into many blocks, with some of them reaching the bottom at t = 0.044 second.

6. CONCLUSION

A second-order manifold method has been described for calculating the distribution of stress and displacement in structures with discontinuities. The process of crack initiation and propagation has been numerically analyzed via both the MM and the singular BEM. The present manifold method is less mesh-dependant than the FEM, and the SIF at the tip of the crack can be predicted very well. Various examples have demonstrated the versatility of this MM for simulating processes involving crack formation and propagation in different structures with discontinuities and the subsequent movement of the component blocks after the structure fails.

Further improvements in the present code will be needed for dealing with crack propagation along any direction. Future studies are also required for simulating fracture problems with pressure stresses at the crack surface and for developing criteria to analyze the second mode fracture problem.

ACKNOWLEDGMENTS: The authors deeply appreciate and kindly acknowledge the valuable suggestions of Dr. Gen Hua Shi and Professor Yuzo Ohnishi.

REFERENCES

1) Shi, G. H.: Manifold method of material analysis, *Proceedings of Ninth Army Conference on Applied Mathematics and Computing, Minnesota,* U.S.A., pp. 51-76, 1991.
2) Shi, G. H.: Manifold Method, *Proceedings of the First International Forum on Discontinuous Deformation Analysis (DDA) and Simulations of Discontinuous Media,* Berkeley, California, USA, pp. 52-204, 1996.
3) Zhang, G. X., Sugiura, Y. and Hasegawa, H.: Crack propagation and thermal fracture analysis by Manifold Method, *Proceedings of the Second International Conference on Analysis of Discontinuous Deformation,* Kyoto, Japan, pp. 282-297, 1997.
4) Zhang, G. X., Sugiura, Y. and Saito, K.: Failure simulation of foundation by manifold method and comparison with experiment, *Journal of Applied Mechanics (JSCE),* Vol. 1, pp.427-436, 1998.
5) Chiou, Y. J., Tsay, R. J. and Chuang, W. L.: Crack propagation using manifold method, *Proceedings of the Second International Conference on Analysis of Discontinuous Deformation,* Kyoto, Japan, pp. 298-308, 1997.
6) Zhang, G. X. and Liu, G. T.: Thermally stressed multiple system in steady state. *Theoret. Fracture Mech.,* Vol. 17, pp. 69-81,1992.
7) Zhang, G. X. and Liu, G. T.: Harmonic thermal fracture of multiple crack system and the stability of cracks in RCC arch dam. *Engng. Fracture Mech.* Vol. 54, No. 5, pp. 653-656, 1996.
8) Chen, Y. Z.: General case of multiple crack problems in infinite plate. *Engng. Fracture Mech.* Vol. 20, pp. 591-598, 1984.
9) Erdogan, F. and Sih, G. C.: On the crack extension in plates under plane loading and transverse shear. ASCE, *J. Basic Engng.* Vol. 85, pp. 519-525, 1963.
10) Yin, S. Z.: Fracture and damage theories and their application, *TsingHua University Press,* Beijing, China, 1992.
11) Murakami, Y.: Stress intensity factor handbook (vol. 1), *Pregamon Books Ltd.,* Great Britain, 1987.

(Received October 21,1997)

マニフォールド法と境界要素法を用いたクラックシミュレーション

張 国新・杉浦 靖人・長谷川 浩夫

本論文は，著者らが改良を加えたマニフォールド法により，クラックの発生と伝達をシミュレーションしたものである．クラック端部の特異性を考慮した境界要素法により，クラックの応力拡大係数と伝達方向を求める．クラックの発生は，モール・クーロン則に従うものとし，ラックの進展は最大周応力方向に進むものとした．本手法を静的および動的問題に適用したいくつかの解析例を紹介する．